

DreamSparse: Escaping from Plato’s Cave with 2D Frozen Diffusion Model Given Sparse Views

Paul Yoo

Jiaxian Guo *

Yutaka Matsuo

Shixiang Shane Gu

The University of Tokyo

pauyoo@weblab.t.u-tokyo.ac.jp

<https://sites.google.com/view/dreamsparse-webpage>

Figure 1: Qualitative results on novel view synthesis of real-world objects from the CO3D dataset.

Abstract

Synthesizing novel view images from a few views is a challenging but practical problem. Existing methods often struggle with producing high-quality results or necessitate per-object optimization in such few-view settings due to the insufficient information provided. In this work, we explore leveraging the strong 2D priors in pre-trained diffusion models for synthesizing novel view images. 2D diffusion models, nevertheless, lack 3D awareness, leading to distorted image synthesis and compromising the identity. To address these problems, we propose *DreamSparse*, a framework that enables the frozen pre-trained diffusion model to generate geometry and identity-consistent novel view image. Specifically, *DreamSparse* incorporates a geometry module designed to capture 3D features from sparse views as a 3D prior. Subsequently, a spatial guidance model is introduced to convert these 3D feature maps into spatial information for the generative process. This information is then used to guide the pre-trained diffusion model, enabling it to generate geometrically consistent images without tuning it. Leveraging the strong image priors in the pre-trained diffusion models, *DreamSparse* is capable of synthesizing high-quality novel views for both object and scene-level images and generalising to open-set images. Experimental results demonstrate that our framework can effectively synthesize novel view images from sparse views and outperforms baselines in both trained and open-set category images. More results can be found on our project page: <https://sites.google.com/view/dreamsparse-webpage>.

*Corresponding Author: Jiaxian Guo (jiaxian.guo@weblab.t.u-tokyo.ac.jp)

1 Introduction

“How could they see anything but the shadows if they were never allowed to move their heads?”

- Plato’s Allegory of the Cave

Plato’s Allegory of the Cave raises a thought-provoking question about our perception of reality. Human perception of 3D objects is often limited to the projection of the world as 2D observations. We rely on our prior experiences and imagination abilities to infer the unseen views of objects from these 2D observations. As such, perception is to some degree a creative process retrieving from imagination. Recently, Neural Radiance Fields (NeRF) [25] exhibited impressive results on novel view synthesis by utilizing implicit functions to represent volumetric density and color data. However, NeRF requires a large amount of images from different camera poses and additional optimizations to model the underlying 3D structure and synthesize an object from a novel view, limiting its use in real-world applications such as AR/VR and autonomous driving. In most practical applications, typically only a few views are available for each object, in which case leads NeRF to output degenerate solutions with distorted geometry [29, 67, 70].

Then recent works [77, 29, 67, 70, 13, 6, 64, 16] started to explore sparse-view novel view synthesis, specifically focusing on generating novel views from a limited number of input images (typically 2-3) with known camera poses. Some of them [29, 67, 70, 13, 6] tried to introduce additional priors into NeRF, *e.g.* depth information, to enhance the understanding of 3D structures in sparse-view scenarios. However, due to the limited information available in few-view settings, these methods struggle to generate clear novel images for unobserved regions. To address this issue, SparseFusion [77] and GenNVS[3] propose learning a diffusion model as an image synthesizer for inferring high-quality novel-view images and leveraging prior information from other images within the same category. Nevertheless, since the diffusion model is only trained within a single category, it faces difficulties in generating objects in unseen categories and needs further distillation for each object, rendering it still impractical.

In this paper, we investigate the utilization of 2D image priors from pre-trained diffusion models, such as Stable Diffusion [37], for generalizable novel view synthesis **without** further per-object training based on sparse views. However, since pre-trained diffusion models are not designed for 3D structures, directly applying them can result in geometrically and textually inconsistent images, compromising the object’s identity in Figure 6. To address this issue, we introduce *DreamSparse*, a framework designed to leverage the 2D image prior from pre-trained diffusion models for novel view image synthesis using a few (2) views. In order to inject 3D information into the pre-trained diffusion model and enable it to synthesize images with consistent geometry and texture, we initially employ a geometry module [54] as a 3D geometry prior inspired by previous geometry-based works [36, 35, 27, 19, 67, 54, 16], which is capable of aggregating feature maps across multi-view context images and learning to infer the 3D features for the novel view image synthesis. This 3D prior allows us to render an estimate from a previously unseen viewpoint while maintaining accurate geometry.

However, due to the modality gap, the extracted 3D features cannot be directly used as the input to the pre-trained diffusion model for synthesizing geometry-consistent novel view images. Alternatively, we propose a spatial guidance module which is able to convert the 3D features into meaningful guidance to change the spatial features [72, 60, 2] in the pre-trained diffusion model, thus enabling the pre-trained diffusion model to generate geometric consistency novel view image [72, 60, 2] without altering its parameters. Nevertheless, the spatial guidance from 3D features alone cannot completely overcome the hallucination problem of the pre-trained models, as the information encoded in 3D features is limited. This means it cannot guarantee identity consistency in synthesised novel view images. To overcome the limitation, we further propose a noise perturbation method, where we denoise the result with the pre-trained diffusion model from the noise added from the blurry novel estimate instead of random ones, so that we can further utilize the identity information from the estimate in 3D geometry model. In this way, the frozen pre-trained diffusion model is able to both effective synthesis high-quality novel view images with consistent geometry and identity.

With the strong image synthesis capacity of the frozen pre-trained diffusion model, our approach offers several benefits: 1) The ability to infer unseen regions of objects without additional training, as pre-trained diffusion models already possess strong image priors learned from large-scale image-text datasets. 2) A strong generalization capability, allowing the generation of images across various categories and even in-the-wild images using the strong image priors in the pre-trained diffusion

models. 3) The ability to synthesize high-quality and even scene-level images without additional per-object optimization. 4) Since we do not modify the parameters or replace the textual embedding [20] of the pre-trained text-to-image diffusion model, the textual control capability of the pre-existing model is preserved. This allows us to alter the style/texture of the synthesized novel view image with textual control. The comparisons with other methods are given in Table 1.

In our experiments, we applied our framework to the real-world CO3D dataset [33]. The extensive qualitative and quantitative results demonstrated that our approach outperformed baselines in both object-level and scene-level novel view synthesis settings by a large margin (about 50% in FID and 20% in LPIPS). Specifically, the results in open-set categories of DreamSparse can even achieve competitive performance with those of the baselines in training domains, demonstrating the advantage of exploiting prior from pre-trained 2D diffusion model in open-set generalization.

Table 1: Comparisons with prior works on 1) works with sparse (2-6) input views, 2) generates geometrically consistent views, 3) hallucinates unseen regions, 4) generalizes to instances in unseen categories because of the pre-trained backbones, and 5) free of training during inference time for novel view synthesis. 6) The ability to edit with textual control.

	RegNeRF[29]	VolSDF[71]	NeRS [70]	IBRNet[64]	NF[33]	LFN[48]	SRT[43]	PixelNeRF[67]	GPNR[54]	VF[16]	3DFuse[46]	SF[77]	Ours
1) Sparse-Views	✓	✓	✓	✗	✓	✓	✓	✓	✗	✓	✓	✓	✓
2) 3D consistent	✓	✓	✓	✓	✓	✓	✓	✓	✓	✗	✓	✓	✓
3) Generate Unseen	✗	✗	✗	✗	✗	✗	✗	✗	✗	✓	✓	✓	✓
4) Open-Set Generalization	✗	✗	✗	✓	✓	✗	✓	✓	✓	✓	✓	✗	✓
5) Train-Free for NVS	✗	✗	✗	✓	✓	✗	✓	✓	✓	✓	✗	✗	✓
6) Textual Control	✗	✗	✗	✗	✗	✗	✗	✗	✗	✗	✓	✗	✓

2 Related Works

Geometry-based Novel View Synthesis. Prior research on Novel View Synthesis (NVS) largely focuses on recovering the 3D structure of a scene. This is achieved by estimating the parameters of the input images’ camera and subsequently applying a multi-view stereo (MVS) technique, as indicated by several studies [52, 44, 9, 1]. These methods use explicit geometry proxies to facilitate NVS. However, it often fails to synthesize novel views that are both photo-realistic and comprehensive, particularly in the case of occluded areas. In order to address this issue, recent strategies [35, 36] have attempted to integrate the 3D geometry derived from an MVS pipeline with NVS approaches based on deep learning. Despite its progress, the overall quality may deteriorate if the MVS pipeline encounters failures. The utilization of other explicit geometric representations has also been explored by various recent NVS techniques. These include the usage of depth maps [8, 59], multi-plane images [7, 75], or voxels [49, 21].

Sparse-view 3D Reconstruction. Novel View Synthesis (NVS) from fewer views aims to generate a new image from a novel viewpoint using a limited number of 2D images [56]. Because of the limited information available in this setting, most works [57, 76, 51, 14, 47, 55] need the per-object or per-category test-time optimization, which makes them impractical. [59, 30, 55, 67, 58, 5, 64, 16, 50, 39, 34, 13, 54] tried to encode observation into incorporate 3D information, by using 3D information, *e.g.*, depth and volume or stronger neural backbone, *e.g.*, transformer [62]. In order to synthesize high-quality novel view images, several recent approaches have utilized diffusion priors, such as 3DiM [65], SparseFusion [77], NeRDi [6], Zero-1-to-3 [20] and GenNVS [3].

Diffusion Model for 3D Reconstruction In order to achieve high-quality novel view synthesis, recent works tried to introduce diffusion model [12, 53, 37, 41, 22, 22, 61, 69, 74, 6, 17, 18, 24, 66, 32, 28, 26] in this area. In the context of novel view synthesis, 3DiM[65] performs novel view synthesis only conditioned on input images and poses without 3D information, so it is hard to generate 3D-consistent images. Then SparseFusion [77] and NVS-Fusion [3] proposed to integrate additional geometric information as training conditions for the diffusion model, thereby enabling the generation of 3D-consistent images. However, due to the absence of strong 2D prior information

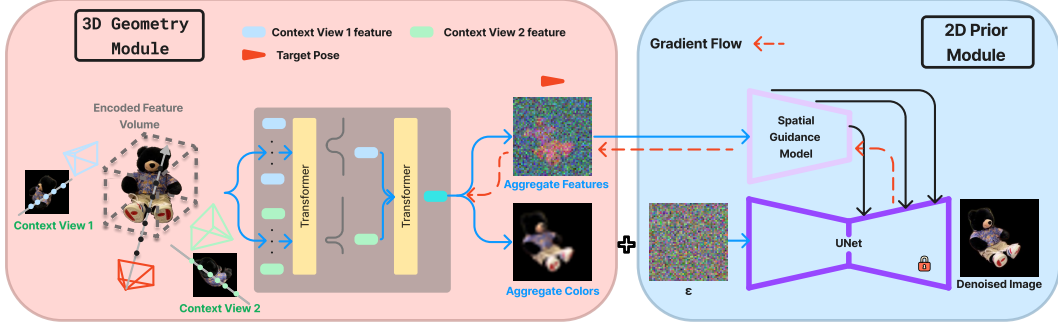


Figure 2: The illustration of the method. The first stage involves utilizing a 3D geometry module to estimate 3D structure and aggregate features from context views. In the next stage, a pre-trained 2D diffusion model conditioned on the aggregate features is leveraged to learn a spatial guidance model that guides the diffusion process for accurate synthesis of the underlying object.

in the diffusion models they employed, these approaches are challenging to generalize to objects in open-set categories. In contrast, our approach utilizes a frozen diffusion model pre-trained on a large-scale dataset [45], enhancing its generalization ability for objects in open-set categories.

3 Method

Given a few context images $\{C_i^{inputs}\}_{i=1}^N$ and their poses π_i , we aim to leverage the 2D image prior from pre-trained diffusion models to synthesize a novel view image at a target pose π_{target} . Because pre-trained diffusion models are not 3D-aware, we first employ a geometry-aware module as a 3D prior to extract features in a 3D volume encoded from given context images. In order to leverage 3D features for the pre-trained diffusion model, we further propose a spatial guidance model to convert geometry-grounded features into spatial features [60, 2] with consistent shape in diffusion models, guiding it to synthesize novel view images with correct geometry. However, we discover that relying solely on the diffusion model to sample an accurate reconstruction from random noise is inadequate at maintaining the object’s identity due to the hallucination problem [15, 32] as shown in 6. Therefore, we propose a noise perturbation method to alleviate it, guiding the diffusion model to synthesise a novel view image with correct geometry and identity. The overall pipeline is illustrated in Fig. 2.

3.1 3D Geometry Module

In order to infuse 3D awareness into 2D diffusion models, we propose a geometry model to extract 3D features with geometric information for 2D diffusion models. In order to obtain geometry grounding, the process begins by casting a query ray from π^{target} and sampling uniformly spaced points along the ray. For each 3D point, we aim to learn density weighting for computing a weighted linear combination of features along the query ray. Subsequently, this per-ray feature is aggregated across multiple context images, yielding a unified perspective on the 3D structure we aim to reconstruct. Lastly, we render a feature map at π^{target} by raycasting from the target view. Next, we will present the details of this model.

Point-wise density weighting for each context image. For each input context image C_i^{inputs} , our geometry model first extracts semantic features using a ResNet50 [10] backbone and then reshapes the encoded feature into a 4 dimensional volumetric representation $V_i \in \mathbb{R}^{c \times d \times h \times w}$, where h and w are the height and width of the feature volume, respectively, d is the depth resolution, and c is the feature dimension. We pixel-align the spatial dimensions of the volume to that of the original input image via bilinear upsampling. To derive benefit from multi-scale feature representation, we draw feature maps from the first three blocks of the backbone and reshape them into volumetric representations capturing the same underlying 3D space. Given a 3D query point p_j along a query ray \mathbf{r}^i , we sample feature vectors from all three scales of feature volumes using trilinear interpolation concatenating them together. To calculate the point-wise density weighting, we employ a transformer [62] with a linear projection layer at last followed by a softmax operation to determine a weighted linear combination of point features, resulting in a per-ray feature vector. Further implementation details are reserved for Appendix.

Aggregate features from different context images. To understand the unified structure of the 3D object, we consolidate information from all given context images. More specifically, we employ an extra transformer, enabling us to dynamically consolidate ray features from a varying number of context images that correlate with each query ray. The final feature map rendering at a query view is constructed by raycasting from the query view and computing per-ray feature vector for each ray. We render the feature map \mathbf{F} at a resolution of $\mathbb{R}^{32 \times 32}$, compositing features sampled from a 3D volume with geometry awareness with respect to the target view. We denote g as the feature map rendering function and \mathbf{F} as the resulting aggregate feature map.

$$\mathbf{F} = g_\phi(\boldsymbol{\pi}^{inputs}, \mathbf{C}^{inputs}, \boldsymbol{\pi}^{target}) \quad (1)$$

where $\mathbf{F} \in \mathbb{R}^{d \times 32 \times 32}$ with $d = 256$, and ϕ is trainable parameters.

Color Estimation To enforce geometric consistency, we directly obtain aggregation weights from the transformer outputs and linearly combine RGB color values drawn from the context images to render a coarse color estimate E at the query view.

$$E = g_{\phi,color}(\boldsymbol{\pi}^{inputs}, \mathbf{C}^{inputs}, \boldsymbol{\pi}^{target}) \quad (2)$$

We impose a color reconstruction loss on the coarse image against the ground-truth image.

$$\mathcal{L}_{recon} = \sum_{\boldsymbol{\pi}^{target}} \|g_{\phi,color}(\boldsymbol{\pi}^{inputs}, \mathbf{C}^{inputs}, \boldsymbol{\pi}^{target}) - C^{target}\|^2 \quad (3)$$

3.2 Spatial Guidance Module

Because of the modality gap between the 3D features \mathbf{F} and the input of the pre-trained diffusion model, 3D features cannot be directly used as the input of the pre-trained diffusion model. To leverage the 3D information in the 3D features, we propose the spatial guidance module to convert the 3D features into guidance to rectify the spatial features [60, 72, 2] that have a role in forming fine-grained spatial information in the diffusion process (normally the feature maps after the 4-th layer). To derive this guidance from 3D features, we construct our spatial guidance module following ControlNet [72] which trains a separate copy of all the encoder blocks as well as the middle block from Stable Diffusion’s U-Net with 1x1 convolution layers initialized with zeros between each block. Let T_θ be the spatial guidance module, and intermediate outputs from each block j of T_θ as $T_{\theta,j}(\mathbf{F})$ with weight λ . In order to change the spatial features in the pre-trained diffusion model, we directly add $T_{\theta,j}(\mathbf{F})$ into the corresponding decoder block of the pre-trained diffusion model’s U-Net. By optimizing T_θ with gradients backpropagated from the pre-trained diffusion model’s noise prediction objective.

$$\mathcal{L}_{diffusion} = \mathbb{E}_{x_0, t, \mathbf{F}, \epsilon \sim \mathcal{N}(0, 1)} \left[\|\epsilon - \epsilon_\psi(x_{t+1}, t, T_\theta(\mathbf{F}))\|^2 \right] \quad (4)$$

T_θ will be optimized to learn how to semantically meaningful convert 3D features from the geometry model into the guidance to rectify spatial features in the diffusion process, enabling it to generate geometry-consistent images. In Section 4.5, we visualize the spatial features after adding the spatial guidance to show the effects of the spatial guidance model. During training, we jointly optimize g_ϕ and T_θ using the overall loss.

$$\min_{\phi, \theta} \mathcal{L}_{recon}(g_\phi) + \mathcal{L}_{diffusion}(T_\theta) \quad (5)$$

While in training time, we use a ground-truth image as x_0 to optimize $\mathcal{L}_{diffusion}$, in inference time, we initialize x_0 with an image rendered from $g_{\phi,color}$.

Noise Perturbation While spatial guidance module by itself is able to guide the pre-trained diffusion model to synthesize novel view images with consistent geometry. It still not always can synthesise images with the same identity as context views because of the hallucinate problem [15, 32] in the pre-trained models. To alleviate this problem, we propose adding noise perturbation to the novel view estimate E from the geometry model and denoising the result with the pre-trained diffusion model, *e.g.* Stable Diffusion [38], so that it can leverage the identity information from the estimate. As shown by [23], applying the denoising procedure can project the sample to a manifold of natural images. We use the formulations from denoising diffusion models [12] to perturb an initial image $x_0 = E$ with Gaussian noise to get a noisy image x_t as follows:

$$x_t = \sqrt{\bar{\alpha}_t}x_0 + \sqrt{1 - \bar{\alpha}_t}\epsilon \quad (6)$$

where $\bar{\alpha}_t$ depends on scheduling hyperparameters and $\epsilon \sim \mathcal{N}(0, 1)$. During the training time, the noise is still randomly initialized, and we use the Noise Perturbation method in the inference time to improve the identity consistency. We show its ablation study in Section 4.5.

4 Experiments

In this section, we first validate the efficacy of our DreamSparse framework on zero-shot novel view synthesis by comparing it with other baselines. Then, we perform ablation studies on important design choices, such as noise perturbation and visualization of spatial features, to understand their effects. We also present qualitative examples of our textual control ability and include a discussion on observations.

4.1 Dataset and Training Details

Following SparseFusion [77], we perform experiments on real-world scenes from the Common Objects in 3D (CO3Dv2) [33], a dataset with real-world objects annotated with camera poses. We train and evaluate our framework on the CO3Dv2 [33] dataset’s `fewview_train` and `fewview_dev` sequence sets respectively. We use Stable Diffusion v1.5 [38] as the frozen pre-trained diffusion model and DDIM [53] to synthesize novel views with 20 denoising steps. The resolutions of the feature map for the spatial guidance module and latent noise are set as 32×32 , and the spatial guidance weight $\lambda = 2$. The three transformers used in the geometry module are all 4 layers, and the output 3D features are set as 32×32 to match the latent noise dimensions. We jointly train the geometry and the spatial models on 8 A100-40GB GPUs for 3 days with a batch size of 15. To demonstrate our model’s generalization capability at object-level novel view synthesis, we trained our framework on a subset of 10 categories as specified in [33]. During each training iteration, a query view and one to four context views of an object were randomly sampled as inputs to the pipeline. To further evaluate scene-level novel view synthesis capability, we trained our framework on the hydrant category, incorporating the full background, using the same training methodology as above.

4.2 Competing Methods

We compare against previous state-of-the-art (SoTA) methods for which open-source code is available. We have included PixelNeRF [68], a feature re-projection method, in our comparison. Additionally, we compare our methods against SparseFusion [77], the most recently published SoTA method that utilizes a diffusion model for NVS. We train our framework and SparseFusion on 10 categories of training sets. The PixelNeRF training was conducted per category due to its category-specific hyperparameters. For a fair comparison, all methods perform NVS **without** per-object optimization during the inference time. Because we do not replace the textual embedding in the pre-trained diffusion model, we use the prompt ‘a picture of <class_name>’ as the default prompt for both training and inference.

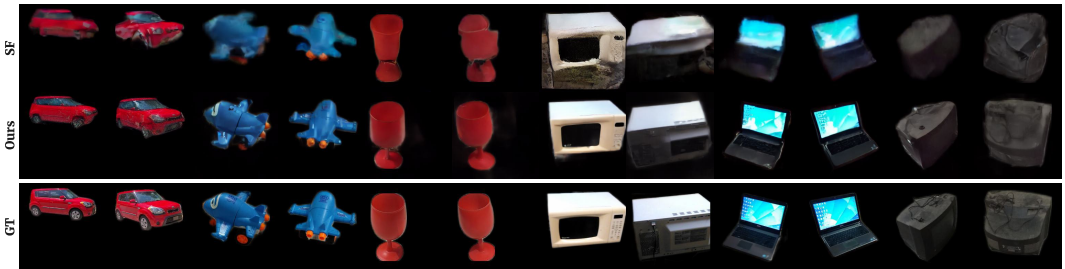


Figure 3: Novel view synthesizing results on **open-set** category objects with the same context image inputs, where SF denotes SparseFusion [77] and GT denotes Ground-Truth image. More results are given at our project webpage and appendix.

4.3 Main Results Analysis

Given 2 context views, we evaluate novel view synthesis quality using the following metrics: FID [11], LPIPS [73], and PSNR². We believe that the combination of FID, LPIPS, and PSNR provides a comprehensive evaluation of novel view synthesis quality. FID and LPIPS measure the perceptual quality of the images, while PSNR measures the per-pixel accuracy. We note that PSNR has some drawbacks as a metric for evaluating generative models. Specifically, PSNR tends to favor blurry

²https://en.wikipedia.org/wiki/Peak_signal-to-noise_ratio

Table 2: Quantitative evaluation metrics on 10 subset of training categories from CO3D, where PN denotes PixelNerf [68] and SF denotes SparseFusion [77]. Limited by the width, we only show FID and LPIPS score here.

	Apple		Ball		Bench		Cake		Donut		Hydrant		Plant		Suitcase		Teddybear		Vase		Avg.	
	FID	LPIPS	FID	LPIPS	FID	LPIPS	FID	LPIPS	FID	LPIPS	FID	LPIPS	FID	LPIPS	FID	LPIPS	FID	LPIPS	FID	LPIPS	FID	LPIPS
PN	247.1	0.57	319.2	0.56	344.0	0.53	380.8	0.58	340.8	0.63	318.7	0.48	335.0	0.52	333.9	0.45	352.1	0.56	288.9	0.47	326.1	0.54
SF	110.9	0.28	143.5	0.30	255.8	0.34	185.7	0.33	126.6	0.29	165.7	0.23	168.5	0.31	202.6	0.28	199.3	0.34	167.8	0.23	172.6	0.29
Ours	42.8	0.19	45.8	0.19	122.5	0.25	105.2	0.23	67.2	0.21	87.8	0.16	86.2	0.23	100.2	0.20	91.2	0.23	69.1	0.16	81.8	0.21

Table 3: Quantitative evaluation on 10 **open-set** categories outside of the training split, where SF denotes SparseFusion [77].

	Bicycle		Car		Couch		Laptop		Microwave		Motorcycle		Bowl		Toyplane		TV		Wineglass		Avg.	
	FID	LPIPS	FID	LPIPS	FID	LPIPS	FID	LPIPS	FID	LPIPS	FID	LPIPS	FID	LPIPS	FID	LPIPS	FID	LPIPS	FID	LPIPS	FID	LPIPS
SF	217.7	0.34	209.5	0.30	201.1	0.44	223.8	0.36	200.4	0.40	205.8	0.35	198.4	0.26	202.2	0.26	261.4	0.33	208.5	0.23	212.9	0.33
Ours	154.7	0.26	116.5	0.22	129.9	0.31	167.3	0.26	127.2	0.29	115.4	0.29	61.9	0.16	98.5	0.19	167.9	0.24	82.7	0.15	122.2	0.24

images that lack detail. This is because PSNR only measures the per-pixel accuracy of an image, and does not take into account the overall perceptual quality of the image. By using all three metrics, we can get a more complete picture of the quality of the images generated by our model.

4.3.1 Object Level Novel View Synthesis

In-Domain Evaluation We evaluate the performance of unseen objects NVS in training 10 categories. The quantitative results are presented in Table 5, which clearly demonstrates that our method surpasses the baseline methods in terms of both FID and LPIPS metrics. More specifically, DreamSparse outperforms SparseFusion by a substantial margin of 53% in the FID score and 28% in LPIPS. This significant improvement can be attributed to DreamSparse’s capacity to generate sharper, semantically richer images, as depicted in Figure 1. This indicates the benefits of utilizing the potent image synthesis capabilities of pre-trained diffusion models.

Open-Set Evaluation We also evaluate the performance of objects NVS in open-set 10 categories, because PixelNerf is per-category trained, we do not report its open-set generalization results. According to Table 6, it is evident that our method surpasses the baseline in both evaluation metrics in all categories, surpassing the second-best method by 28% in LPIPS and 43% in FID. Moreover, the results derived from our method are not just competitive, but can even be compared favourably to the training category evaluations of the baseline in Table 5 (122.2 vs 172.2 in FID and 0.24 vs 0.29 in LPIPS). This clearly illustrates the benefits of utilizing 2D priors from a large-scale, pre-trained 2D diffusion model for open-set generalization. We also show the qualitative results in Figure 3, and it shows that the novel view image synthesised by our method can still achieve sharp and meaningful results on objects in open-set categories.

4.3.2 Scene Level Novel View Synthesis

We report our evaluation results about scene-level NVS in Table 7. As shown in the table, DreamSparse significantly outperforms the baselines in terms of FID and LPIPS scores, surpassing the second-best performance by approximately 70% in FID and 24% in LPIPS, respectively. This underscores the effectiveness of our method in the context of scene-level NVS tasks. Despite our method showing comparable performance to the baseline in terms of Peak Signal-to-Noise Ratio (PSNR), it’s worth mentioning that PSNR often favors blurry images lacking in detail [42, 40, 3]. This becomes evident in Figure 4, where despite our sharp and consistent synthesis results, PSNR still leans towards the blurry image produced by PixelNeRF.

Table 4: Quantitative evaluation metrics for scene-level novel view synthesis on the hydrant category from CO3D, where SF denotes SparseFusion [77].

	1 View			2 Views			5 Views		
	FID↓	LPIPS↓	PSNR↑	FID↓	LPIPS↓	PSNR↑	FID↓	LPIPS↓	PSNR↑
PixelNeRF [68]	343.89	0.75	13.31	319.96	0.74	13.94	286.30	0.71	14.59
SparseFusion [77]	272.72	0.81	13.05	255.05	0.78	13.55	231.73	0.71	14.91
Ours	75.63	0.59	13.02	73.47	0.56	13.48	70.62	0.54	14.15

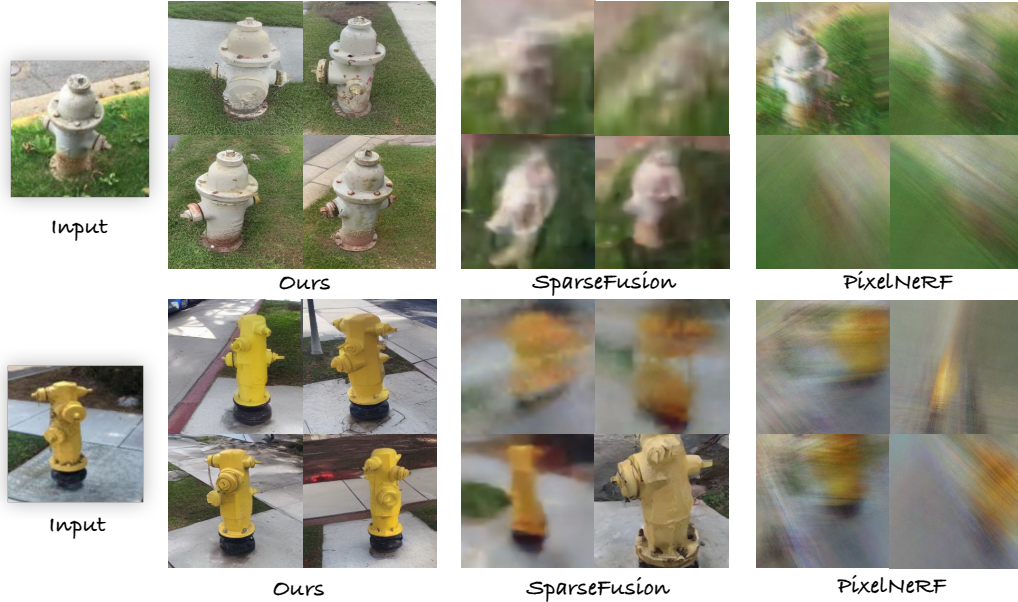
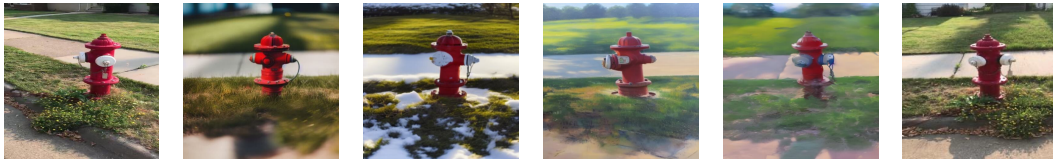


Figure 4: Qualitative results of scene-level novel view synthesis (NVS) outputs from all baselines.

4.4 Textual Control Style Transfer

As we do not replace or remove text conditioning in the pre-trained diffusion model, our method is additionally capable of controlling the image generation with text. We demonstrate an example use case where we conduct both novel view synthesis and style transfer via text in Figure 5.



Context +Photograph +Snow +Oil Painting +Monet GT

Figure 5: Qualitative results of novel view synthesis with textual control style transfer

4.5 Ablation Studies



Figure 6: Effect of the spatial guidance weighting of spatial guidance signals at the residual connections in the middle and decoder blocks of the diffusion model.

Number of Input Views We investigate the performance by varying the number of context view inputs. The results are depicted in Table 6, which clearly illustrates the enhancement of three evaluation metrics as the number of input views increases. Moreover, the performance disparity between the **single view** and multiple input views is less pronounced in our method than in other baselines - a 6% difference vs 14% difference in Sparse Fusion vs a 17% difference in PixelNeRF. This observation leads to two key conclusions: 1) DreamSparse exhibits greater robustness in response to variations in the number of context view inputs. 2) Despite the decrease in performance, DreamSparse can efficiently synthesise novel views from a single input view.

Spatial Feature Visualization To investigate the impact of the spatial guidance model, we employ Principal Component Analysis (PCA) [31] to visualize the spatial features post-integration of spatial guidance following [60]. As shown in Figure 7, the visualized feature maps from the 2nd, 3rd, and 4th blocks of the UNet decoder indicate that despite the contextual view's geometry varying from that of the novel view, the feature maps steered by our spatial guidance model maintain alignment with



Figure 7: The spatial feature visualization with spatial guidance model, where context denotes the input context image, 2nd block denotes the visualization of feature maps from the 2nd block of the decoder and output denotes the synthesised novel view image.

the geometry of the ground truth image. This consistency enables the pre-trained diffusion model to generate images that accurately mirror the original geometry.

Spatial Guidance Weight We investigate the effects of spatial guidance weight on the quality and consistency of synthesised novel view images. Our study varies the spatial guidance weight λ , and the results in Fig 6 showed that when $\lambda = 0$ (indicating no spatial guidance), the pre-trained diffusion model failed to synthesise a novel view image that was consistent in terms of geometry and identity. However, as the weight increased, the synthesised images exhibited greater consistency with the ground truth. It is important to note, though, that an excessively high weight could diminish the influence of features in the pre-trained diffusion model, potentially leading to blurry output. Given the trade-off between quality and consistency, we set $\lambda = 2$ as the default hyperparameter.

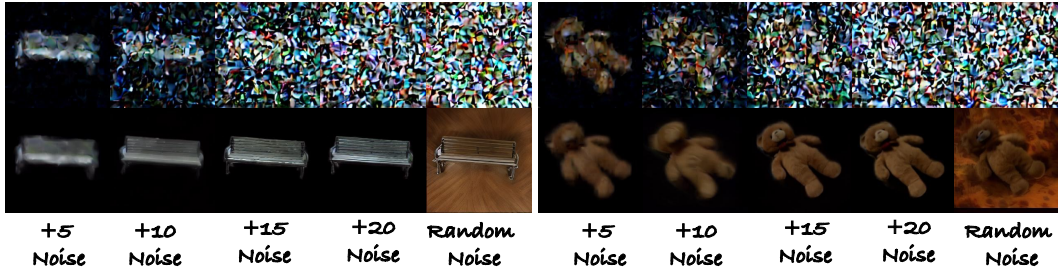


Figure 8: Effect of noise perturbation level on novel view image synthesis. The images in the top row are visualizations of noised images as input to the diffusion process, and the images in the bottom row are the synthesized images from diffusion model. +5 noise denotes the addition of 5 steps of noise to the color estimate from the geometry model, and random noise denotes randomly sampled Gaussian noise. All images were generated using a DDIM [53] sampler with 20 inference steps.

Effect of Noise Perturbing Color Estimation The impact of the Noise Perturbation method is showcased in Figure 8. It is evident that when the diffusion process begins from random noise, the spatial guidance model can successfully guide the pre-trained diffusion model to synthesize images with consistent geometry. However, the color or illumination density information is partially lost, leading to distortions in the synthesized novel view. In contrast, synthesizing the image from noise that is added to the color estimation in the geometry model yields better results. As depicted in ‘+20 Noise’ in Figure 8, the pre-trained diffusion model can effectively utilize the color information in the estimates, resulting in a more consistent image synthesis. We also experimented with varying the noise level added to the estimate. Our observations suggest that if the noise added to the blurry estimation is insufficient, the pre-trained diffusion model struggles to denoise the image because of the distribution mismatch between the blurry color estimate and Gaussian distribution, thereby failing to produce a sharp and consistent output.

5 Conclusion

In this paper, we present the *DreamSparse* framework, which leverages the strong 2D priors of a frozen pre-trained text-to-image diffusion model for novel view synthesis from sparse views. Our method outperforms baselines in both training and open-set object-level novel view synthesis. Our technique surpasses existing benchmarks in both the training and the open-set object-level novel view synthesis. Further results corroborate the benefits of utilizing a pre-trained diffusion model in scene-level NVS as well as in the generation of text-controlled scenes style transfer, clearly outperforming existing models and demonstrating the potential of leveraging the 2D pre-trained diffusion models for novel view synthesis.

Limitations and Negative Social Impact Despite its capabilities, we discovered that our 3D Geometry Module struggles with generating complex scenes, especially ones with non-standard

geometry or intricate details. This is due to the limited capacity of the geometry module and limited data, and we will introduce a stronger geometry backbone and train it on larger datasets. On the social impact front, our technology could potentially lead to job displacement in certain sectors. For instance, professionals in fields such as graphic design or 3D modelling might find their skills becoming less in demand as AI-based techniques become more prevalent and advanced. It’s important to note that these negative implications are not exclusive to this study, and should be widely considered and addressed within the realm of AI research.

References

- [1] Sameer Agarwal, Yasutaka Furukawa, Noah Snavely, Ian Simon, Brian Curless, Steven M Seitz, and Richard Szeliski. Building rome in a day. *Communications of the ACM*, 54(10):105–112, 2011.
- [2] Dmitry Baranchuk, Ivan Rubachev, Andrey Voynov, Valentin Khrukov, and Artem Babenko. Label-efficient semantic segmentation with diffusion models. *arXiv preprint arXiv:2112.03126*, 2021.
- [3] Eric R Chan, Koki Nagano, Matthew A Chan, Alexander W Bergman, Jeong Joon Park, Axel Levy, Miika Aittala, Shalini De Mello, Tero Karras, and Gordon Wetzstein. Generative novel view synthesis with 3d-aware diffusion models. *arXiv preprint arXiv:2304.02602*, 2023.
- [4] Angel X Chang, Thomas Funkhouser, Leonidas Guibas, Pat Hanrahan, Qixing Huang, Zimo Li, Silvio Savarese, Manolis Savva, Shuran Song, Hao Su, et al. Shapenet: An information-rich 3d model repository. *arXiv preprint arXiv:1512.03012*, 2015.
- [5] Anpei Chen, Zexiang Xu, Fuqiang Zhao, Xiaoshuai Zhang, Fanbo Xiang, Jingyi Yu, and Hao Su. Mvsnerf: Fast generalizable radiance field reconstruction from multi-view stereo. In *Proceedings of the IEEE/CVF International Conference on Computer Vision*, pages 14124–14133, 2021.
- [6] Congyue Deng, Chiyu Jiang, Charles R Qi, Xinchun Yan, Yin Zhou, Leonidas Guibas, Dragomir Anguelov, et al. Nerdi: Single-view nerf synthesis with language-guided diffusion as general image priors. *arXiv preprint arXiv:2212.03267*, 2022.
- [7] John Flynn, Michael Broxton, Paul Debevec, Matthew DuVall, Graham Fyffe, Ryan Overbeck, Noah Snavely, and Richard Tucker. Deepview: View synthesis with learned gradient descent. In *Proceedings of the IEEE/CVF Conference on Computer Vision and Pattern Recognition*, pages 2367–2376, 2019.
- [8] John Flynn, Ivan Neulander, James Philbin, and Noah Snavely. Deepstereo: Learning to predict new views from the world’s imagery. In *Proceedings of the IEEE conference on computer vision and pattern recognition*, pages 5515–5524, 2016.
- [9] Michael Goesele, Noah Snavely, Brian Curless, Hugues Hoppe, and Steven M Seitz. Multi-view stereo for community photo collections. In *2007 IEEE 11th International Conference on Computer Vision*, pages 1–8. IEEE, 2007.
- [10] Kaiming He, Xiangyu Zhang, Shaoqing Ren, and Jian Sun. Deep residual learning for image recognition. In *Proceedings of the IEEE conference on computer vision and pattern recognition*, pages 770–778, 2016.
- [11] Martin Heusel, Hubert Ramsauer, Thomas Unterthiner, Bernhard Nessler, and Sepp Hochreiter. Gans trained by a two time-scale update rule converge to a local nash equilibrium. *Advances in neural information processing systems*, 30, 2017.
- [12] Jonathan Ho, Ajay Jain, and Pieter Abbeel. Denoising diffusion probabilistic models. *arXiv preprint arxiv:2006.11239*, 2020.
- [13] Ajay Jain, Matthew Tancik, and Pieter Abbeel. Putting nerf on a diet: Semantically consistent few-shot view synthesis. In *Proceedings of the IEEE/CVF International Conference on Computer Vision (ICCV)*, pages 5885–5894, October 2021.
- [14] Wonbong Jang and Lourdes Agapito. Codenerf: Disentangled neural radiance fields for object categories. In *Proceedings of the IEEE/CVF International Conference on Computer Vision*, pages 12949–12958, 2021.
- [15] Ziwei Ji, Nayeon Lee, Rita Frieske, Tiezheng Yu, Dan Su, Yan Xu, Etsuko Ishii, Ye Jin Bang, Andrea Madotto, and Pascale Fung. Survey of hallucination in natural language generation. *ACM Computing Surveys*, 55(12):1–38, 2023.
- [16] Jonáš Kulháněk, Erik Derner, Torsten Sattler, and Robert Babuška. Viewformer: Nerf-free neural rendering from few images using transformers. In *European Conference on Computer Vision (ECCV)*, 2022.

- [17] Gang Li, Heliang Zheng, Chaoyue Wang, Chang Li, Changwen Zheng, and Dacheng Tao. 3ddesigner: Towards photorealistic 3d object generation and editing with text-guided diffusion models. *arXiv preprint arXiv:2211.14108*, 2022.
- [18] Ting-Hsuan Liao, Ge Songwei, Xu Yiran, Yao-Chih Lee, AlBahar Badour, and Jia-Bin Huang. Text-driven visual synthesis with latent diffusion prior. *arXiv preprint arXiv:*, 2023.
- [19] David B Lindell, Dave Van Veen, Jeong Joon Park, and Gordon Wetzstein. Bacon: Band-limited coordinate networks for multiscale scene representation. In *Proceedings of the IEEE/CVF Conference on Computer Vision and Pattern Recognition*, pages 16252–16262, 2022.
- [20] Ruoshi Liu, Rundi Wu, Basile Van Hoorick, Pavel Tokmakov, Sergey Zakharov, and Carl Vondrick. Zero-1-to-3: Zero-shot one image to 3d object. *arXiv preprint arXiv:2303.11328*, 2023.
- [21] Stephen Lombardi, Tomas Simon, Jason Saragih, Gabriel Schwartz, Andreas Lehrmann, and Yaser Sheikh. Neural volumes: Learning dynamic renderable volumes from images. *arXiv preprint arXiv:1906.07751*, 2019.
- [22] Shitong Luo and Wei Hu. Diffusion probabilistic models for 3d point cloud generation. In *Proceedings of the IEEE/CVF Conference on Computer Vision and Pattern Recognition (CVPR)*, June 2021.
- [23] Chenlin Meng, Yutong He, Yang Song, Jiaming Song, Jiajun Wu, Jun-Yan Zhu, and Stefano Ermon. Sdedit: Guided image synthesis and editing with stochastic differential equations. In *International Conference on Learning Representations*, 2021.
- [24] Gal Metzer, Elad Richardson, Or Patashnik, Raja Giryes, and Daniel Cohen-Or. Latent-nerf for shape-guided generation of 3d shapes and textures. *arXiv preprint arXiv:2211.07600*, 2022.
- [25] Ben Mildenhall, Pratul P Srinivasan, Matthew Tancik, Jonathan T Barron, Ravi Ramamoorthi, and Ren Ng. Nerf: Representing scenes as neural radiance fields for view synthesis. *Communications of the ACM*, 65(1):99–106, 2021.
- [26] Norman Müller, Yawar Siddiqui, Lorenzo Porzi, Samuel Rota Bulò, Peter Kotschieder, and Matthias Nießner. Diffrrf: Rendering-guided 3d radiance field diffusion. *arXiv preprint arXiv:2212.01206*, 2022.
- [27] Thomas Müller, Alex Evans, Christoph Schied, and Alexander Keller. Instant neural graphics primitives with a multiresolution hash encoding. *ACM Transactions on Graphics (ToG)*, 41(4):1–15, 2022.
- [28] Gimin Nam, Mariem Khelifi, Andrew Rodriguez, Alberto Tono, Linqi Zhou, and Paul Guerrero. 3d-ldm: Neural implicit 3d shape generation with latent diffusion models. *arXiv preprint arXiv:2212.00842*, 2022.
- [29] Michael Niemeyer, Jonathan T Barron, Ben Mildenhall, Mehdi SM Sajjadi, Andreas Geiger, and Noha Radwan. Regnerf: Regularizing neural radiance fields for view synthesis from sparse inputs. In *Proceedings of the IEEE/CVF Conference on Computer Vision and Pattern Recognition*, pages 5480–5490, 2022.
- [30] Simon Niklaus, Long Mai, Jimei Yang, and Feng Liu. 3d ken burns effect from a single image. *ACM Transactions on Graphics (ToG)*, 38(6):1–15, 2019.
- [31] Karl Pearson. Liii. on lines and planes of closest fit to systems of points in space. *The London, Edinburgh, and Dublin philosophical magazine and journal of science*, 2(11):559–572, 1901.
- [32] Ben Poole, Ajay Jain, Jonathan T. Barron, and Ben Mildenhall. Dreamfusion: Text-to-3d using 2d diffusion. *arXiv*, 2022.
- [33] Jeremy Reizenstein, Roman Shapovalov, Philipp Henzler, Luca Sbordone, Patrick Labatut, and David Novotny. Common objects in 3d: Large-scale learning and evaluation of real-life 3d category reconstruction. In *International Conference on Computer Vision*, 2021.
- [34] Jeremy Reizenstein, Roman Shapovalov, Philipp Henzler, Luca Sbordone, Patrick Labatut, and David Novotny. Common objects in 3d: Large-scale learning and evaluation of real-life 3d category reconstruction. In *Proceedings of the IEEE/CVF International Conference on Computer Vision*, pages 10901–10911, 2021.
- [35] Gernot Riegler and Vladlen Koltun. Free view synthesis. In *Computer Vision—ECCV 2020: 16th European Conference, Glasgow, UK, August 23–28, 2020, Proceedings, Part XIX 16*, pages 623–640. Springer, 2020.
- [36] Gernot Riegler and Vladlen Koltun. Stable view synthesis. In *Proceedings of the IEEE/CVF Conference on Computer Vision and Pattern Recognition*, pages 12216–12225, 2021.
- [37] Robin Rombach, Andreas Blattmann, Dominik Lorenz, Patrick Esser, and Björn Ommer. High-resolution image synthesis with latent diffusion models, 2021.
- [38] Robin Rombach, Andreas Blattmann, Dominik Lorenz, Patrick Esser, and Björn Ommer. High-resolution image synthesis with latent diffusion models. In *Proceedings of the IEEE/CVF Conference on Computer Vision and Pattern Recognition*, pages 10684–10695, 2022.

- [39] Robin Rombach, Patrick Esser, and Björn Ommer. Geometry-free view synthesis: Transformers and no 3d priors, 2021.
- [40] Chitwan Saharia, William Chan, Huiwen Chang, Chris Lee, Jonathan Ho, Tim Salimans, David Fleet, and Mohammad Norouzi. Palette: Image-to-image diffusion models. In *ACM SIGGRAPH 2022 Conference Proceedings*, pages 1–10, 2022.
- [41] Chitwan Saharia, William Chan, Saurabh Saxena, Lala Li, Jay Whang, Emily Denton, Seyed Kamyar Seyed Ghasemipour, Burcu Karagol Ayan, S Sara Mahdavi, Rapha Gontijo Lopes, et al. Photorealistic text-to-image diffusion models with deep language understanding. *arXiv preprint arXiv:2205.11487*, 2022.
- [42] Chitwan Saharia, Jonathan Ho, William Chan, Tim Salimans, David J Fleet, and Mohammad Norouzi. Image super-resolution via iterative refinement. *IEEE Transactions on Pattern Analysis and Machine Intelligence*, 2022.
- [43] Mehdi SM Sajjadi, Henning Meyer, Etienne Pot, Urs Bergmann, Klaus Greff, Noha Radwan, Suhani Vora, Mario Lučić, Daniel Duckworth, Alexey Dosovitskiy, et al. Scene representation transformer: Geometry-free novel view synthesis through set-latent scene representations. In *Proceedings of the IEEE/CVF Conference on Computer Vision and Pattern Recognition*, pages 6229–6238, 2022.
- [44] Johannes L Schonberger and Jan-Michael Frahm. Structure-from-motion revisited. In *Proceedings of the IEEE conference on computer vision and pattern recognition*, pages 4104–4113, 2016.
- [45] Christoph Schuhmann, Romain Beaumont, Richard Vencu, Cade Gordon, Ross Wightman, Mehdi Cherti, Theo Coombes, Aarush Katta, Clayton Mullis, Mitchell Wortsman, et al. Laion-5b: An open large-scale dataset for training next generation image-text models. *arXiv preprint arXiv:2210.08402*, 2022.
- [46] Junyoung Seo, Wooseok Jang, Min-Seop Kwak, Jaehoon Ko, Hyeonsu Kim, Junho Kim, Jin-Hwa Kim, Jiyoung Lee, and Seungryong Kim. Let 2d diffusion model know 3d-consistency for robust text-to-3d generation. *arXiv preprint arXiv:2303.07937*, 2023.
- [47] Vincent Sitzmann, Eric Chan, Richard Tucker, Noah Snavely, and Gordon Wetzstein. Metasdf: Meta-learning signed distance functions. *Advances in Neural Information Processing Systems*, 33:10136–10147, 2020.
- [48] Vincent Sitzmann, Semon Rezchikov, Bill Freeman, Josh Tenenbaum, and Fredo Durand. Light field networks: Neural scene representations with single-evaluation rendering. *Advances in Neural Information Processing Systems*, 34:19313–19325, 2021.
- [49] Vincent Sitzmann, Justus Thies, Felix Heide, Matthias Nießner, Gordon Wetzstein, and Michael Zollhofer. Deepvoxels: Learning persistent 3d feature embeddings. In *Proceedings of the IEEE/CVF Conference on Computer Vision and Pattern Recognition*, pages 2437–2446, 2019.
- [50] Vincent Sitzmann, Michael Zollhofer, and Gordon Wetzstein. Scene representation networks: Continuous 3d-structure-aware neural scene representations. In H. Wallach, H. Larochelle, A. Beygelzimer, F. d'Alché-Buc, E. Fox, and R. Garnett, editors, *Advances in Neural Information Processing Systems*, volume 32. Curran Associates, Inc., 2019.
- [51] Vincent Sitzmann, Michael Zollhöfer, and Gordon Wetzstein. Scene representation networks: Continuous 3d-structure-aware neural scene representations. *Advances in Neural Information Processing Systems*, 32, 2019.
- [52] Noah Snavely, Steven M Seitz, and Richard Szeliski. Photo tourism: exploring photo collections in 3d. In *ACM siggraph 2006 papers*, pages 835–846. 2006.
- [53] Jiaming Song, Chenlin Meng, and Stefano Ermon. Denoising diffusion implicit models. *arXiv:2010.02502*, October 2020.
- [54] Mohammed Suhail, Carlos Esteves, Leonid Sigal, and Ameesh Makadia. Generalizable patch-based neural rendering. In *Computer Vision–ECCV 2022: 17th European Conference, Tel Aviv, Israel, October 23–27, 2022, Proceedings, Part XXXII*, pages 156–174. Springer, 2022.
- [55] Matthew Tancik, Ben Mildenhall, Terrance Wang, Divi Schmidt, Pratul P Srinivasan, Jonathan T Barron, and Ren Ng. Learned initializations for optimizing coordinate-based neural representations. In *Proceedings of the IEEE/CVF Conference on Computer Vision and Pattern Recognition*, pages 2846–2855, 2021.
- [56] M. Tatarchenko, A. Dosovitskiy, and T. Brox. Multi-view 3d models from single images with a convolutional network. In *European Conference on Computer Vision (ECCV)*, 2016.
- [57] Maxim Tatarchenko, Alexey Dosovitskiy, and Thomas Brox. Multi-view 3d models from single images with a convolutional network. In *Computer Vision–ECCV 2016: 14th European Conference, Amsterdam, The Netherlands, October 11–14, 2016, Proceedings, Part VII 14*, pages 322–337. Springer, 2016.

- [58] Alex Trevithick and Bo Yang. Grf: Learning a general radiance field for 3d representation and rendering. In *Proceedings of the IEEE/CVF International Conference on Computer Vision*, pages 15182–15192, 2021.
- [59] Richard Tucker and Noah Snavely. Single-view view synthesis with multiplane images. In *Proceedings of the IEEE/CVF Conference on Computer Vision and Pattern Recognition*, pages 551–560, 2020.
- [60] Narek Tumanyan, Michal Geyer, Shai Bagon, and Tali Dekel. Plug-and-play diffusion features for text-driven image-to-image translation. *arXiv preprint arXiv:2211.12572*, 2022.
- [61] Michał J Tyszkiewicz, Pascal Fua, and Eduard Trulls. Gecco: Geometrically-conditioned point diffusion models. *arXiv preprint arXiv:2303.05916*, 2023.
- [62] Ashish Vaswani, Noam Shazeer, Niki Parmar, Jakob Uszkoreit, Llion Jones, Aidan N Gomez, Lukasz Kaiser, and Illia Polosukhin. Attention is all you need. *Advances in neural information processing systems*, 30, 2017.
- [63] Naveen Venkat, Mayank Agarwal, Maneesh Singh, and Shubham Tulsiani. Geometry-biased transformers for novel view synthesis. *arXiv preprint arXiv:2301.04650*, 2023.
- [64] Qianqian Wang, Zhicheng Wang, Kyle Genova, Pratul P Srinivasan, Howard Zhou, Jonathan T Barron, Ricardo Martin-Brualla, Noah Snavely, and Thomas Funkhouser. Ibrnet: Learning multi-view image-based rendering. In *Proceedings of the IEEE/CVF Conference on Computer Vision and Pattern Recognition*, pages 4690–4699, 2021.
- [65] Daniel Watson, William Chan, Ricardo Martin-Brualla, Jonathan Ho, Andrea Tagliasacchi, and Mohammad Norouzi. Novel view synthesis with diffusion models. *arXiv preprint arXiv:2210.04628*, 2022.
- [66] Jiale Xu, Xintao Wang, Weihao Cheng, Yan-Pei Cao, Ying Shan, Xiaohu Qie, and Shenghua Gao. Dream3d: Zero-shot text-to-3d synthesis using 3d shape prior and text-to-image diffusion models. *arXiv preprint arXiv:2212.14704*, 2022.
- [67] Alex Yu, Vickie Ye, Matthew Tancik, and Angjoo Kanazawa. pixelnerf: Neural radiance fields from one or few images. In *Proceedings of the IEEE/CVF Conference on Computer Vision and Pattern Recognition*, pages 4578–4587, 2021.
- [68] Alex Yu, Vickie Ye, Matthew Tancik, and Angjoo Kanazawa. pixelNeRF: Neural radiance fields from one or few images. In *CVPR*, 2021.
- [69] Xiaohui Zeng, Arash Vahdat, Francis Williams, Zan Gojcic, Or Litany, Sanja Fidler, and Karsten Kreis. Lion: Latent point diffusion models for 3d shape generation. In *Advances in Neural Information Processing Systems (NeurIPS)*, 2022.
- [70] Jason Zhang, Gengshan Yang, Shubham Tulsiani, and Deva Ramanan. Ners: neural reflectance surfaces for sparse-view 3d reconstruction in the wild. *Advances in Neural Information Processing Systems*, 34:29835–29847, 2021.
- [71] Kai Zhang, Fujun Luan, Zhengqi Li, and Noah Snavely. Iron: Inverse rendering by optimizing neural sdfs and materials from photometric images. In *Proceedings of the IEEE/CVF Conference on Computer Vision and Pattern Recognition*, pages 5565–5574, 2022.
- [72] Lvmin Zhang and Maneesh Agrawala. Adding conditional control to text-to-image diffusion models. *arXiv preprint arXiv:2302.05543*, 2023.
- [73] Richard Zhang, Phillip Isola, Alexei A Efros, Eli Shechtman, and Oliver Wang. The unreasonable effectiveness of deep features as a perceptual metric. In *Proceedings of the IEEE conference on computer vision and pattern recognition*, pages 586–595, 2018.
- [74] Linqi Zhou, Yilun Du, and Jiajun Wu. 3d shape generation and completion through point-voxel diffusion. In *Proceedings of the IEEE/CVF International Conference on Computer Vision (ICCV)*, pages 5826–5835, October 2021.
- [75] Tinghui Zhou, Richard Tucker, John Flynn, Graham Fyffe, and Noah Snavely. Stereo magnification: Learning view synthesis using multiplane images. *arXiv preprint arXiv:1805.09817*, 2018.
- [76] Tinghui Zhou, Shubham Tulsiani, Weilun Sun, Jitendra Malik, and Alexei A Efros. View synthesis by appearance flow. In *Computer Vision—ECCV 2016: 14th European Conference, Amsterdam, The Netherlands, October 11–14, 2016, Proceedings, Part IV 14*, pages 286–301. Springer, 2016.
- [77] Zhizhuo Zhou and Shubham Tulsiani. Sparsefusion: Distilling view-conditioned diffusion for 3d reconstruction. In *CVPR*, 2023.

We will release our code and pre-trained models upon acceptance of our paper. To enhance visual presentation, we have showcased more qualitative samples on our paper’s website. <https://sites.google.com/view/dreamsparse-webpage>. Next, we present the details of our method and additional quantitative comparisons with a recent baseline GBT and an ablation study on the 3D geometry prior module.

A Method Implementation Details

Feature Extraction Backbone. To encode a volumetric feature field, we input a context image through a ResNet50 [10] backbone and extract multi-scale feature maps from the first three blocks having feature dimensions 256, 512, and, 1024 respectively. To accommodate an additional depth dimension, the feature dimension is divided by the depth, which we set to 64, resulting in features of size 4, 8, 16 for the three volumes respectively. The final feature vector at a query 3D point is a concatenation of features from all three volume scales, making the final feature vector dimension 28.

Weighting Points Along a Ray. We employ a Transformer [62] to learn weightings for computing a linear combination of features of points along a given query ray. To form the input sequence for the Transformer, we follow the input parameterization of [54]. For each point, we concatenate the final feature vector from the backbone with an encoding of the query point and depth along the ray as a positional cue. The query point encoding is computed by first extracting relative poses for all context views with respect to the target view and representing the ray from each context camera origin to the query point in Plücker coordinates. The depth of each point along the ray is additionally parameterized by a sinusoidal positional encoding as in [25]. The output sequence of the Transformer is followed by a linear projection layer and a Softmax operation to yield scalar densities for computing a weighted sum of output features corresponding to points on a query ray.

Multi-view Aggregation Transformer. Once per-ray feature aggregate for each context view has been computed, we similarly learn to combine across all context views via a Transformer. We again concatenate per-ray feature vector output from the previous step with the same Plücker parameterization of query point and sinusoidal positional encoding of depth. All hidden and output dimensions of the Transformers are set to 256.

B Table Update with PSNR and an Additional Baseline

For completeness, we make an addition to the quantitative results to reflect PSNR measurements. Furthermore, we include another baseline GBT [63], a geometry-biased Transformer-based method for novel view synthesis from sparse context views, that demonstrates robust results on 10 categories of CO3D. Although GBT achieves comparable PSNR across training and open-set categories, synthesized novel views tend to be blurry especially for open-set categories and thus underperforming in FID and LPIPS.

Table 5: Quantitative evaluation metrics on 10 subset of training categories from CO3D, where PN denotes PixelNerf [68], SF denotes SparseFusion [77], and Geom Prior is the geometry prior module from our method.

	Apple			Ball			Bench			Cake			Donut			Hydrant		
	FID ↓	LPIPS ↓	PSNR ↑	FID ↓	LPIPS ↓	PSNR ↑	FID ↓	LPIPS ↓	PSNR ↑	FID ↓	LPIPS ↓	PSNR ↑	FID ↓	LPIPS ↓	PSNR ↑	FID ↓	LPIPS ↓	PSNR ↑
PN	247.1	0.57	14.76	319.2	0.56	14.25	344.0	0.53	15.16	380.8	0.58	15.10	340.8	0.63	15.76	318.7	0.48	15.20
GBT	168.85	0.27	22.96	175.18	0.28	21.45	324.28	0.33	19.10	264.86	0.32	20.71	209.33	0.29	22.78	237.22	0.23	21.82
SF	110.9	0.28	20.91	143.5	0.30	20.25	255.8	0.34	17.21	185.7	0.33	19.39	126.6	0.29	20.62	165.7	0.23	19.35
Ours (Geom Prior)	123.98	0.33	22.96	134.41	0.33	22.09	238.95	0.38	19.42	197.00	0.35	21.41	162.12	0.34	22.95	211.03	0.26	21.90
Ours	42.8	0.19	23.72	45.8	0.19	23.12	122.5	0.25	18.68	105.2	0.23	21.73	67.2	0.21	22.88	87.8	0.16	21.71

	Plant			Suitcase			Teddybear			Vase			Avg.		
	FID ↓	LPIPS ↓	PSNR ↑	FID ↓	LPIPS ↓	PSNR ↑	FID ↓	LPIPS ↓	PSNR ↑	FID ↓	LPIPS ↓	PSNR ↑	FID ↓	LPIPS ↓	PSNR ↑
PN	335.0	0.52	18.08	333.9	0.45	20.12	352.1	0.56	14.85	288.9	0.47	15.91	326.1	0.54	15.91
GBT	254.74	0.29	21.29	283.38	0.28	23.41	294.84	0.32	19.93	255.22	0.26	22.28	246.79	0.29	21.57
SF	168.5	0.31	19.60	202.6	0.28	21.87	199.3	0.34	18.03	167.8	0.23	21.36	172.6	0.29	19.85
Ours (Geom Prior)	206.21	0.35	21.64	210.56	0.30	23.69	223.82	0.36	20.68	204.06	0.27	22.74	191.21	0.33	21.95
Ours	86.2	0.23	20.59	100.2	0.20	23.30	91.2	0.23	20.51	69.1	0.16	23.03	81.8	0.21	22.03

Table 6: Quantitative evaluation on 10 **open-set** categories outside of the training split, where SF denotes SparseFusion [77].

	Bicycle			Car			Couch			Laptop			Microwave			Motorcycle		
	FID ↓	LPIPS ↓	PSNR ↑	FID ↓	LPIPS ↓	PSNR ↑	FID ↓	LPIPS ↓	PSNR ↑	FID ↓	LPIPS ↓	PSNR ↑	FID ↓	LPIPS ↓	PSNR ↑	FID ↓	LPIPS ↓	PSNR ↑
SF	217.7	0.34	17.57	209.5	0.30	17.49	201.1	0.44	19.25	223.8	0.36	18.73	200.4	0.40	17.65	205.8	0.35	17.52
GBT	259.77	0.33	19.10	287.64	0.33	18.18	272.82	0.43	20.10	276.15	0.36	19.75	276.44	0.41	17.40	294.84	0.35	18.50
Ours (Geom Prior)	235.36	0.38	19.39	218.86	0.34	19.11	182.56	0.39	21.58	231.58	0.39	21.09	213.55	0.45	19.26	259.89	0.41	18.65
Ours	154.7	0.26	18.16	116.5	0.22	18.38	129.9	0.31	20.36	167.3	0.26	20.13	127.2	0.29	18.96	115.4	0.29	17.35

	Bowl			Toyplane			TV			Wineglass			Avg.		
	FID ↓	LPIPS ↓	PSNR ↑	FID ↓	LPIPS ↓	PSNR ↑	FID ↓	LPIPS ↓	PSNR ↑	FID ↓	LPIPS ↓	PSNR ↑	FID ↓	LPIPS ↓	PSNR ↑
SF	198.4	0.26	19.08	202.2	0.26	18.81	261.4	0.33	22.58	208.5	0.23	19.21	212.9	0.33	18.79
GBT	246.56	0.27	20.94	270.80	0.26	19.85	337.60	0.34	22.78	266.84	0.24	21.36	278.94	0.27	20.94
Ours (Geom Prior)	172.42	0.32	21.11	204.66	0.33	21.18	252.78	0.37	23.98	224.73	0.26	21.21	219.64	0.36	20.66
Ours	61.9	0.16	22.30	98.5	0.19	20.53	167.9	0.24	23.65	82.7	0.15	22.08	122.2	0.24	20.19

C Ablation Study for Geometry Model

We further evaluate novel view image estimates from the stand-alone geometry model alongside other baselines. From Tables 5, 6, 7, we observe the geometry model outperforming the full version of our method in terms of PSNR in many cases. This is a consequence of the geometry model often rendering blurry coarse images as the view deviates from the context images. As PSNR, being a measurement favoring lower mean squared error across pixels, encourages mean pixel color, blurry images tend to score higher. However, significant drops in FID and LPIPS indicate lower image quality and perceptual dissimilarity, highlighting the importance of the 2D prior module in imagining missing details.

Table 7: Quantitative evaluation metrics for scene-level novel view synthesis on the hydrant category from CO3D.

	1 View			2 Views			5 Views		
	FID ↓	LPIPS ↓	PSNR ↑	FID ↓	LPIPS ↓	PSNR ↑	FID ↓	LPIPS ↓	PSNR ↑
PixelNeRF [68]	343.89	0.75	13.31	319.96	0.74	13.94	286.30	0.71	14.59
SparseFusion [77]	272.72	0.81	13.05	255.05	0.78	13.55	231.73	0.71	14.91
Ours (Geom Prior)	322.46	0.70	14.53	279.16	0.65	15.37	216.34	0.57	17.16
Ours	75.63	0.59	13.02	73.47	0.56	13.48	70.62	0.54	14.15

D Evaluation Setup

For computing evaluation metrics, we select 10 objects per category and sample 32 uniformly spaced camera poses from the held-out test split. We then randomly select a specified number of context views from the camera poses and evaluate novel view synthesis results on the rest of the poses.

E Additional Training and Evaluation on ShapeNet

We additionally train and evaluate our method and baselines on the cars category of the ShapeNet [4] synthetic dataset of object renderings. We train all methods on 2458 training car objects each containing 50 views. We randomly sample 1 to 3 context views during training. For evaluation, we randomly pick 10 objects from the test set with 251 views per object. We randomly sample one context view and evaluate on all other novel views. The final metrics are averaged across all views and objects. Quantitative results in Table 8 show improvements in FID and LPIPS over other baselines, indicating sharper image quality and diversity in synthesized results in comparison to the image distribution of ShapeNet cars and more faithful structure and texture of novel view reconstructions.

Table 8: Quantitative evaluation metrics for ShapeNet [4] cars category. For all baselines, only a single context view was provided as input to compute the metrics over novel views.

	FID↓	LPIPS↓	PSNR↑
PixelNeRF [68]	154.96	0.14	23.32
SparseFusion [77]	127.61	0.19	19.82
Ours	101.86	0.13	20.29